



# Adsorption of dyes in aqueous solutions by chitosan–halloysite nanotubes composite hydrogel beads



Qi Peng, Mingxian Liu\*, Jianwen Zheng, Changren Zhou\*

Department of Materials Science and Engineering, Jinan University, Guangzhou 510632, PR China

## ARTICLE INFO

### Article history:

Received 18 June 2014

Received in revised form 13 August 2014

Accepted 1 September 2014

Available online 16 September 2014

### Keywords:

Nanotube

Composite

Adsorption

Interactions

Adsorption kinetics

## ABSTRACT

Composite hydrogel beads containing chitosan and halloysite nanotubes (HNTs) with a well defined structure were prepared by the dropping and pH-precipitation method. The influence of HNTs on the appearance, diameter, microstructures, and thermal stability of the chitosan beads was characterized. The composite hydrogels exhibit slightly increased diameter and improved thermal stability. A rough surface and high concentration of the nanotubes in the bead core are found in the composite beads. The hydrogel beads were employed as adsorbents for removal of methylene blue and malachite green from aqueous solutions and the fundamental adsorption behavior was studied. Both Langmuir isotherm and Freundlich isotherm models can fit the isotherm adsorption data well. The addition of HNTs can significantly increase the adsorption rate of chitosan beads for the two dyes. Moreover, with the increase of the amount of hydrogel beads in the dye solution, the removal ratio of dyes increases but the absorption amount per unit adsorbent weight gradually reduces. The adsorption kinetics closely follows pseudo-second order model. The regeneration experimental shows that the adsorption ability of all the beads can be recovered especially for methylene blue. So the chitosan–HNTs composite hydrogels can be potentially used for the removal of dyes from wastewater.

© 2014 Elsevier Inc. All rights reserved.

## 1. Introduction

It is important to find an effective way of dyes pollution treatment for our environment, because dyes are harmful to human beings and toxic to microorganisms [1]. The dyes can cause the decrease of water transmittance and hinder the growth of bacteria and other micro-organisms simultaneously. Furthermore, the dyes can disturb the aquatic photosynthesis and damage the ecosystem [2,3]. To address this problem, various natural or synthesized materials have been used for treatment of the wastewater by adsorption of the dyes.

Chitosan, a cationic polysaccharide, contains amino groups and hydroxyl groups, which generates strong adsorption and complexation interactions with dyes via the hydrogen bonding, electrostatic attraction, ion exchange and van der Waals force, etc [4–6]. The adsorption types include physical adsorption, chemical adsorption and ion exchange adsorption, so chitosan-based adsorbent materials can absorb all kinds of dye molecules [7,8]. Although chitosan has many advantages as an adsorbent for dyes wastewater [9–15], the dye adsorption amount and adsorption rate of chitosan needs to be further improved for practical applications [16].

One routine for solving this problem is to design and prepare chitosan nanocomposites. There are strong interactions between chitosan and nanoparticles [17–20], which is responsible for the enhancement of the adsorption properties. For example, the adsorption performance of chitosan hydrogel beads was improved by the incorporation of multiwalled carbon nanotubes (MWNTs) for removal of congo red [21]. Graphene oxide (GO) was added into the porous spongy chitosan by the freeze-drying method. The chitosan–GO composite sponges could be used as adsorbents for methyl orange and  $\text{Cu}^{2+}$  ions [22]. Chitosan intercalated montmorillonite (Chi-MMT) was prepared by Monvisade et al. and the adsorption capacities of Chi-MMT for all basic dyes increased [23]. Copello et al. synthesized chitosan composite hydrogels by adding  $\text{SiO}_2$  hybrid mesoporous materials via the sol–gel method, and the prepared composites had potential applications as biosorbents [24].

Halloysite is a clay mineral composed of myriad thin tubular or fibrous crystals, which is a product by weathering and depositing [25–27]. The application of halloysite is similar to that of kaolinite, including ceramic raw materials, catalysis, and polymer nanofillers. Halloysite shows short tubular structures with high aspect ratio (ca. 20), thus it is usually called as “halloysite nanotubes (HNTs)” [28]. HNTs are widely used in the areas of electronics, catalysis, biological and functional materials due to their

\* Corresponding authors. Fax: +86 (20) 85223271.

E-mail addresses: [liumx@jnu.edu.cn](mailto:liumx@jnu.edu.cn) (M. Liu), [tcz9@jnu.edu.cn](mailto:tcz9@jnu.edu.cn) (C. Zhou).

submicron hollow tubular structure, rich reactive groups, and large surface/volume ratio [29]. Compared with other tubular nanomaterials (such as carbon nanotubes (CNTs)), natural HNTs are cheap and environmentally friendly [30–32]. Due to these excellent properties, HNTs can be used as cheap and efficient adsorbents for dyes wastewater (such as methylene blue) [32,33]. However, the direct application of HNTs powder as dye adsorbent is limited, since HNTs will swell and form a highly stable colloidal suspension upon contacting with water, making their separation from water very difficult. In addition, the use of HNTs powder as an adsorbent material in columns is limited due to the low permeability of the compacted HNTs [34]. As a result, constructing composite bead adsorbent by combining HNTs and biopolymers is critical for practical applications, since they exhibit improved mechanical strength and dye adsorption performance.

The individual features of chitosan and HNTs have inspired us the feasibility of combining them to make an effective composite material for dyes removal. Based on the interactions between chitosan and HNTs [35,36], this work prepared chitosan–HNTs composite hydrogel beads by the dropping and pH-precipitation method [37,38]. The influence of HNTs on appearances, size, microstructure, thermal stability of the chitosan was investigated firstly. Methylene blue and malachite green were selected as models to evaluate the capacity of chitosan–HNTs hydrogel beads for the removal of dyes from aqueous solutions [39,40]. This work provides a novel routine for preparing dye adsorption materials by simple fabrication method with high performance as well as low cost.

## 2. Experimental

### 2.1. Raw materials

Chitosan (CS) was supplied by Jinan Haidebei Marine Bioengineering Co. Ltd (China). The deacetylation and viscosity-average molecular weight were 95% and 600,000 g mol<sup>-1</sup> respectively. Halloysite was mined from Hunan province, China. Before using, halloysite was purified according to the reference [27]. The elemental composition of purified HNTs by X-ray fluorescence (XRF) was determined as follows (wt.%): SiO<sub>2</sub>, 54.29; Al<sub>2</sub>O<sub>3</sub>, 44.51; Fe<sub>2</sub>O<sub>3</sub>, 0.63; TiO<sub>2</sub>, 0.006. The Brunauer–Emmett–Teller (BET) surface area of HNTs was 50.4 m<sup>2</sup> g<sup>-1</sup>. Methylene blue (MB) and malachite green (MG) were analytical grade and used as received without further purification (Scheme 1). Ultrapure water from Arium 611 Ultrapure Water Systems (Sartorius, Germany) was used to prepare the aqueous solutions.

### 2.2. Preparation of chitosan–HNTs composite hydrogel beads by using dropping and pH-precipitation method

The pure chitosan and chitosan–HNTs composite hydrogel beads were prepared by the dropping and pH-precipitation method. The procedure was as follows: 2 g chitosan powder and

2 mL acetic acid were added to 100 mL deionized water. By stirring for 6 h, 2 wt.% chitosan solution was prepared. Then 0.5, 1, 2, 4 g HNTs powder was added into the solution under stirring for 6 h to obtain homogeneously dispersed chitosan–HNTs dispersion. The drop-wise addition of the dispersions into a precipitation bath containing 1 mol L<sup>-1</sup> NaOH solution under mild stirring gave rise to the chitosan–HNTs composite hydrogel beads. Pure chitosan bead was prepared with similar procedure but without addition of HNTs. The beads were extensively washed with deionized water and preserved in an aqueous environment for future use. The weight ratio of chitosan and HNTs was 2:1, 1:1, 1:2, 1:4, and which was referred to CS2N1, CS1N1, CS1N2, and CS1N4, respectively.

### 2.3. Structure characterization of chitosan–HNTs composite hydrogel beads

#### 2.3.1. Determining the diameter of the hydrogel beads

The diameters of the hydrogel beads were determined by using the optical microscope. At least, 100 beads were tested for every group and the averages were calculated.

#### 2.3.2. Scanning electronic microscopy (SEM)

The hydrogel beads were soaked in ethanol solution and dried under room temperature. Afterward, the samples were cut by using a blade to observe the structures using of SEM (Ultra55, ZEISS).

#### 2.3.3. Thermogravimetric analysis (TGA)

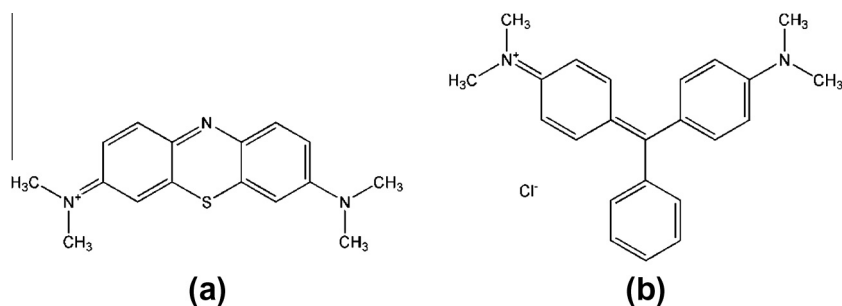
TGA of the dried chitosan and chitosan–HNTs hydrogels was carried out with a NETZSCH TG 209 F3 Tarsus<sup>®</sup> from 30 °C to 600 °C at a heating rate of 10 °C min<sup>-1</sup> under N<sub>2</sub> atmosphere. This experiment was used to study the thermal degradation behavior of the hydrogel beads.

### 2.4. Dyes adsorption properties of chitosan–HNTs hydrogel beads

Batch adsorption experiments were conducted and equilibrated using a thermostatic shaker bath operated at 90 rpm at room temperature (30 °C). All adsorption experiments were repeated at least three to ensure accuracy of the obtained data. The dye concentrations in the solutions were determined at the wavelength of 630 nm by using MK3 microplate reader (THERMO LABSYSTEM, USA). The amount of MB and MG adsorbed on hydrogel was calculated by the following equation:

$$q_e = \frac{(C_0 - C_e)V}{W} \quad (1)$$

where  $q_e$  is the amount of dye adsorbed onto the unit amount of the hydrogel (mg g<sup>-1</sup>),  $c_0$  is the initial concentration of dye (mg L<sup>-1</sup>),  $c_e$  is the final or equilibrium concentration of dye (mg L<sup>-1</sup>),  $V$  is the volume of the dye solution (L) and  $W$  is the weight of hydrogel bead (g).



Scheme 1. Chemical structures of methylene blue (a) and malachite green (b).

The equilibrium isotherm was determined by placing the hydrogel beads into a series of MB solutions (5 mL) with concentrations ranged from 0.04 to 0.24 g L<sup>-1</sup> or MG solution (2 mL) with concentrations ranged from 0.45 to 1.05 g L<sup>-1</sup>. The remaining amount of dyes in the aqueous solution was then determined at 24 h for MB and 14 day for MG (far above the adsorption equilibrium time).

The adsorption kinetics was analyzed by placing the hydrogel beads into 5 mL 0.16 g L<sup>-1</sup> MB solution or 2 mL 0.75 g L<sup>-1</sup> MG solution. For the adsorption kinetics, three kinetic models, namely, the pseudo-first-order, pseudo-second order, and intra-particle diffusion were carried out to fit the experimental data.

The influence of adsorbent dosage on dyes adsorption was examined by adding 0.002–0.01 g hydrogel beads into 5 mL 0.16 g L<sup>-1</sup> MB solution or 2 mL 0.75 g L<sup>-1</sup> MG solution.

### 2.5. Desorption and reusability experiments

0.5 mol L<sup>-1</sup> NaOH aqueous solution and acetone were selected to desorb MB and MG dyes absorbed on the hydrogel beads respectively. After removing the beads from the desorption medium, the dye concentrations were determined by MK3 microplate reader at the wavelength of 630 nm. The regenerated hydrogel beads were placed into 5 mL 0.16 g L<sup>-1</sup> MB solution or 2 mL 0.75 g L<sup>-1</sup> MG solution again. When absorption equilibrium reached, the remaining amount of dyes was determined.

## 3. Results and discussion

### 3.1. Appearance and diameter of chitosan–HNTs composite hydrogel beads

Fig. 1 shows the appearance of prepared wet and dried hydrogel beads. It can be seen that the transparency of hydrogel beads is

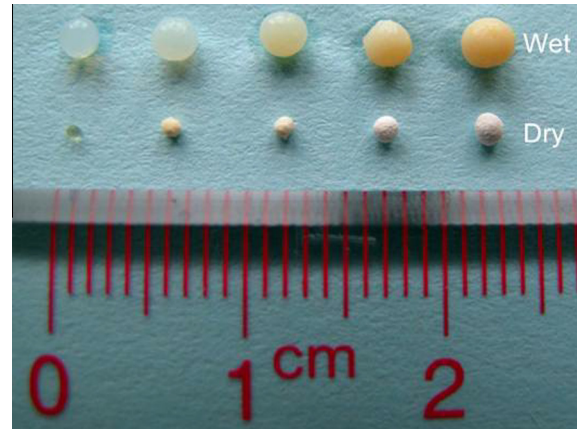


Fig. 1. Appearance of chitosan and chitosan–HNTs hydrogel beads in wet and dry state.

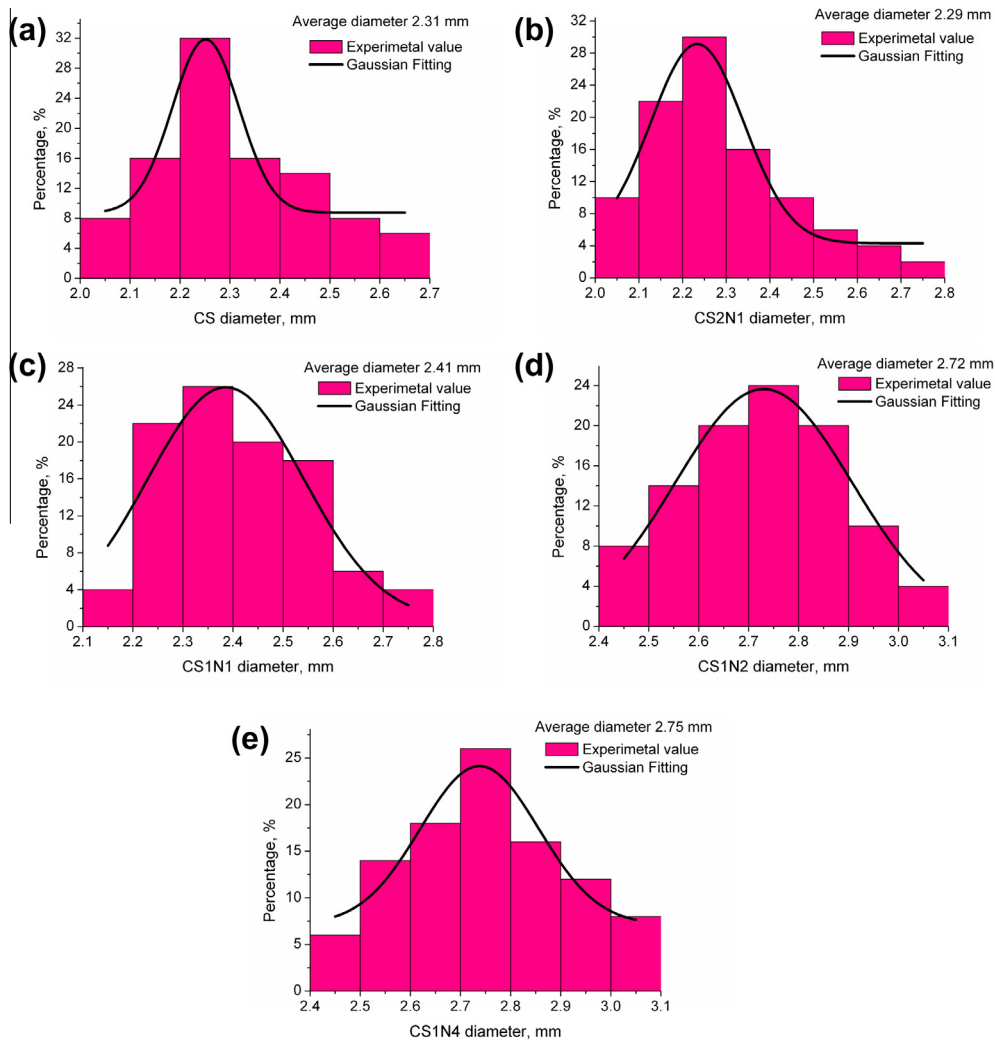


Fig. 2. Diameter of CS, CS2N1, CS1N1, CS1N2, CS1N4 wet hydrogel beads.

reduced upon the addition of HNTs [37]. For dried beads, the larger proportion of HNTs in the composite is, the more significant white color for the beads displays. All the wet beads are spherically shaped with smooth surface, while a noticeable reduced size is observed after drying. The increasing trend of size for chitosan–HNTs composite hydrogel beads is more remarkable in the dried state, because the composite beads have more materials content compared with the pure chitosan bead. The drops of the aqueous chitosan–HNTs dispersion in contact with the alkali solution do not generate opalescence, suggesting that HNTs are immobilized by chitosan hydrogel and fully incorporated into the beads' structure [34,37]. Meanwhile, the hardness of hydrogel beads increases by HNTs via hand touching the beads.

Fig. 2 shows the diameter distribution of the prepared wet hydrogel beads. All the samples show normal particle size distribu-

tion. The average diameter of the hydrogel beads ranges from 2.29 to 2.75 mm. There is a slightly increased trend in bead size with the HNTs loadings. The change of average particle diameter is related to the viscosity variation of the dispersion [35]. Due to the increased viscosity, the composites beads show greater diameter than that of pure chitosan beads. Previous reports showed that the size of composite hydrogel beads composed of chitosan and laponite [41] or alginate–HNTs [37] was not affected by the addition of the nanoclay.

### 3.2. Microstructure of chitosan–HNTs composite hydrogel beads

To investigate the influence of HNTs on the microstructures of the dried chitosan bead, SEM observation was conducted [42]. As shown in Fig. 3, the pure chitosan bead exhibits smooth outer

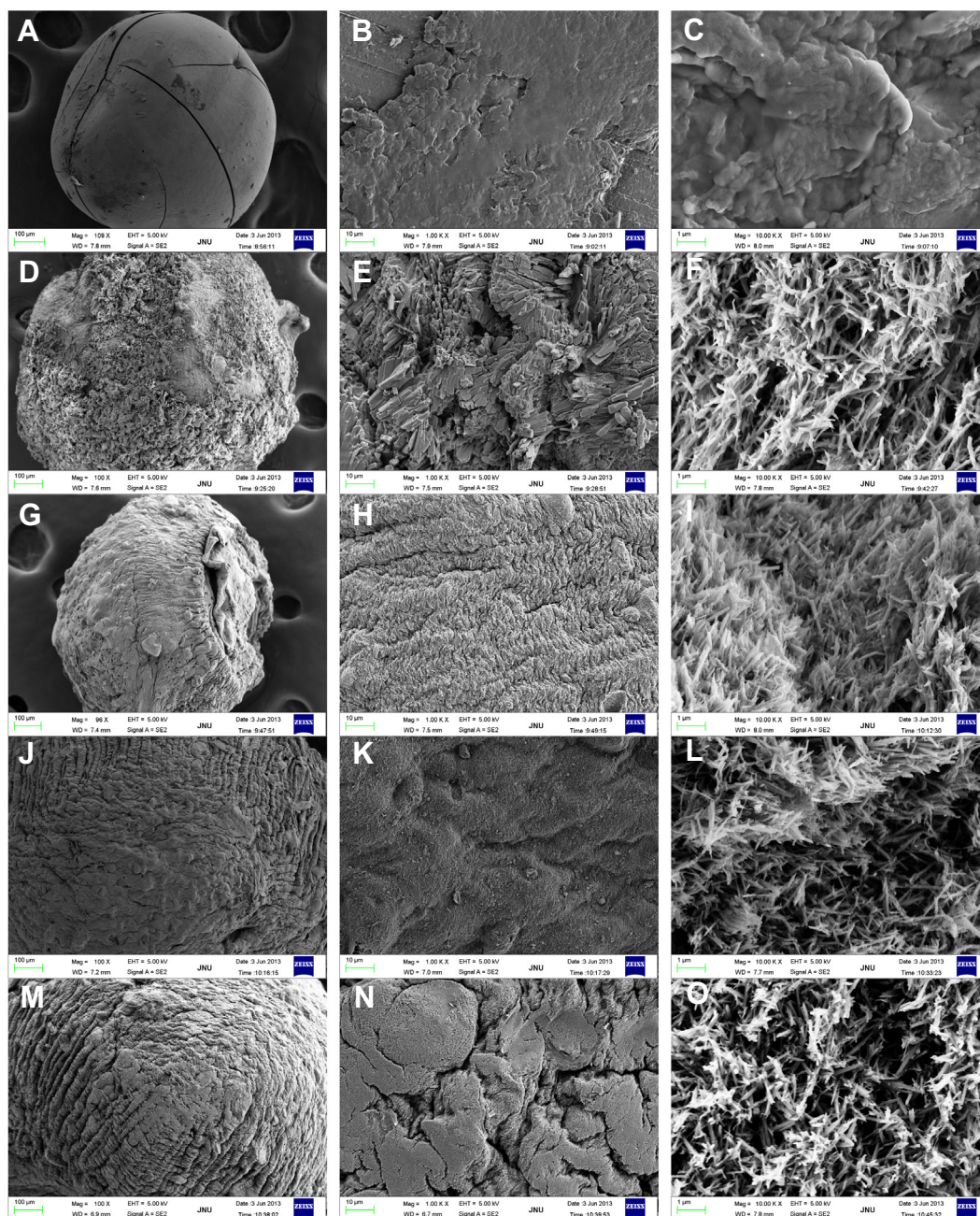


Fig. 3. Internal (C, F, I, L and O) and external (A, B, D, E, G, H, J, K, M and N) structure of chitosan–HNTs hydrogel beads. The concentration of HNTs is gradually increased from top to bottom.

(Fig. 3A and B) and inner (Fig. 3C) surface, indicating the uniform structure. For the composite beads with HNTs, the outer surface (Fig. 3D, G, J and M) is much rougher, while the inside of composite hydrogel beads contains a large number of HNTs (Fig. 3F, I, L and O). HNTs are disordered and coated with chitosan, suggesting that HNTs are immobilized fully by chitosan hydrogel beads inside. In addition, the nanotubes also appear at the bead outer surface (Fig. 3E, H, K and N). When investigating the core structure of the dried hydrogel beads, the HNTs are more numerous than those at the peel. This can be explained by the fact that the formation of the hydrogel beads is attributed to the pH-precipitation of chitosan solution. The large surface area and the loosen structure of the composite hydrogel beads are favorable to molecular diffusion and provide sufficient space for adsorption of dyes [34].

### 3.3. TG analysis of chitosan–HNTs composite hydrogel beads

The thermal stability of the chitosan and chitosan–HNTs hydrogel beads was studied by TG analysis (Fig. 4). From the TG curves, the most obvious stage of decomposition is at  $\sim 270^\circ\text{C}$ , which is assigned to the degradation of the chitosan chains. The summary of the TGA results are shown in Table 1. The temperature at maximum weight loss rate for hydrogel beads of different proportions is related to chitosan component. With the addition of HNTs, the residual weight at  $600^\circ\text{C}$  of composite evidently increases. The temperature at 5% weight loss for pure chitosan is  $66^\circ\text{C}$ . While this temperature for the composite hydrogel beads with 33 wt.% HNTs increases to  $146^\circ\text{C}$ , which is  $80^\circ\text{C}$  higher than that of pure chitosan beads. When 80 wt.% HNTs are added, this temperature further increases to  $173^\circ\text{C}$ . The temperature at 20% weight loss shows a

similar trend. Thus HNTs can enhance the thermal stability of chitosan adsorbents. Enhancement of thermal stability is attributed to two reasons. Char formation occurs at the expense of volatiles and the char itself act as a barrier and hinder diffusion of volatile loss [43]. The char residue content of chitosan–HNT composites is higher than pure chitosan (Table 1). Therefore, the chitosan–HNTs composites can improve the thermal stability compared with pure chitosan. On the other hand, there are hydrogen bonding and electrostatic attraction interactions [36] between chitosan and HNTs. The interfacial interactions also facilitate the enhancement of the thermal stability of the polymers [44,45]. From the TGA results we can conclude that chitosan and HNTs are compatible and the thermal stability of chitosan is improved by the addition of HNTs.

### 3.4. Adsorption isotherms

Both chitosan and HNTs possess abundant hydroxyl groups and unique microstructures which can adsorb dyes by various kinds of interactions. The MB adsorption isotherms for chitosan and chitosan–HNTs hydrogel beads are presented in Fig. 5. The MB absorption on CS, CS1N1, and CS1N4 hydrogel beads increases rapidly with the increase of the dye concentration until 9, 8, and  $7\text{ mg L}^{-1}$ , respectively. When the dye concentration continues to increase, the increasing trend of  $q_e$  slows down due to the saturation of the active sites of the adsorbent. The  $q_e$  values for the MB solutions absorbed by the composite hydrogel beads are higher than those of pure chitosan beads, suggesting the increased absorption ability by the incorporation of HNTs.

Two common isotherm models for adsorption were used to fit experimental data. Langmuir isotherm model is based on the assumption that adsorption sites are identical and energetically equivalent, and only monolayer adsorption occurs in the process [46]. It is mathematically described as follows:

$$\frac{1}{q_e} = \frac{1}{q_{\max}} + \frac{1}{q_{\max}b} \frac{1}{C_e} \quad (2)$$

where  $q_{\max}$  ( $\text{mg g}^{-1}$ ) represents the maximum uptake of MB and  $b$  ( $\text{L mg}^{-1}$ ) is the constant related to the energy of adsorption.  $q_{\max}$  and  $b$  can be determined from the linear plot of  $q_e^{-1}$  versus  $C_e^{-1}$ .

Freundlich isotherm model is based on the assumption of exponentially decaying adsorption site energy distribution [47]. It is used for heterogeneous surface energy systems and can be given as follows:

$$\ln q_e = \frac{1}{n} \ln C_e + \ln K_F \quad (3)$$

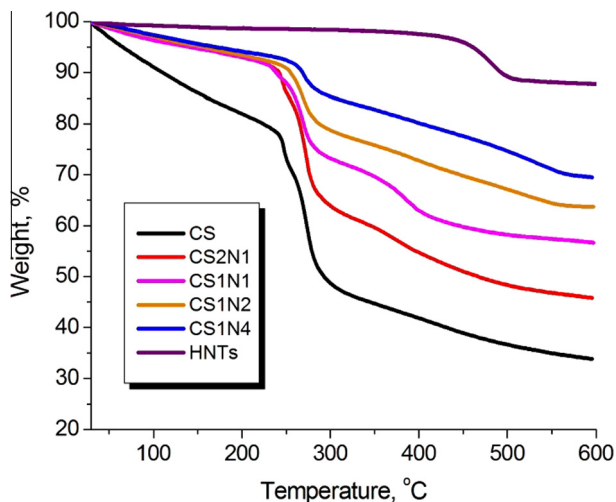


Fig. 4. TG curves for CS, HNTs and CS–HNTs hydrogel beads.

Table 1  
Summary of the TGA results for CS, HNTs and CS–HNTs hydrogel beads.

HNTs composition (w/w%)	Temperature at 5% weight loss ( $^\circ\text{C}$ )	Temperature at 20% weight loss ( $^\circ\text{C}$ )	Remaining weight (%)	Temperature at maximum weight loss rate ( $^\circ\text{C}$ )
0	66	226	34	273
33	146	266	46	271
50	143	271	57	268
67	157	288	64	268
80	173	405	70	270
100	461	–	88	483

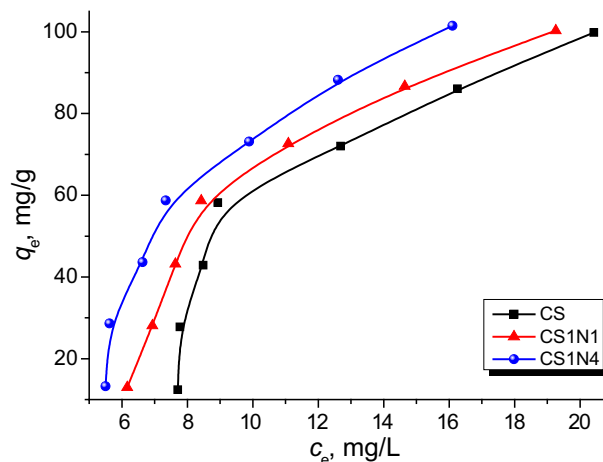


Fig. 5. Adsorption isotherms of MB on CS and CS–HNTs hydrogel beads at 303 K.

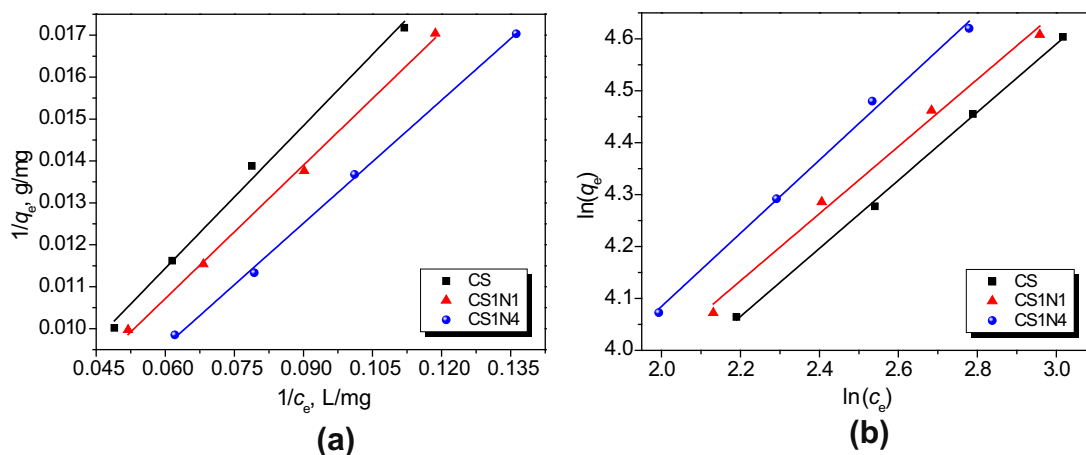


Fig. 6. Langmuir isotherms (a) and Freundlich isotherms (b) for MB adsorption on CS and CS-HNTs hydrogel beads.

Table 2

Langmuir and Freundlich parameters for MB adsorption into chitosan and chitosan-HNTs composites.

Sample	Langmuir parameters			Freundlich parameters		
	$q_{\max}$ ( $\text{mg g}^{-1}$ )	$b$ ( $\text{L mg}^{-1}$ )	$R^2$	$1/n$	$K_F$ ( $\text{mg g}^{-1}$ )	$R^2$
CS	217.39	0.0406	0.9924	0.6564	13.75	0.9984
CS1N1	232.56	0.0406	0.9973	0.6470	15.03	0.9893
CS1N4	270.27	0.0378	0.9985	0.7049	14.51	0.9946

where  $K_F$  is the constant that stands for adsorption capacity related to bond strength and  $1/n$  is a constant indicating adsorption intensity.  $K_F$  and  $n$  can be determined from the linear plot of  $\ln q_e$  versus  $\ln c_e$ .

Fig. 6 shows Langmuir isotherms (a) and Freundlich isotherms (b) of hydrogel beads for MB adsorption. The theoretical isotherm parameters,  $q_{\max}$ ,  $b$ ,  $K_F$ ,  $n$  and the correlation coefficients ( $R^2$ ) are listed in Table 2. It is found that the adsorption of all the beads is well fitted both models. It is revealed that CS1N1 and CS1N4 exhibit higher adsorption capacity than pure CS for MB in the aqueous solution. Also, the calculated value of  $q_{\max}$  increases with the adding of HNTs. Meanwhile, all the samples have a  $1/n$  value within 0.5–1, indicating that the prepared hydrogel beads are good adsorbents for MB [48].

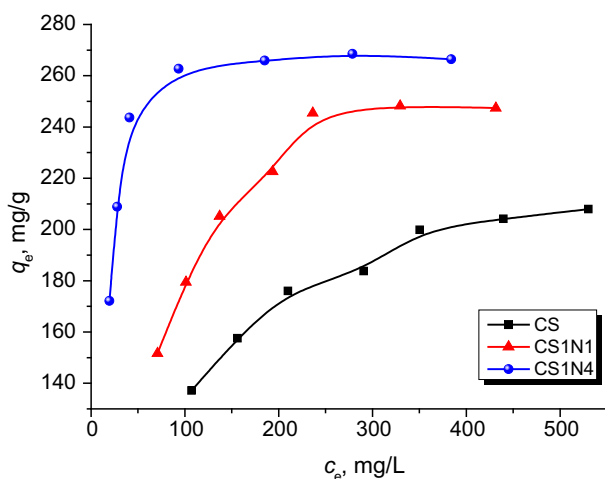


Fig. 7. Adsorption isotherms of MG on CS and CS-HNTs hydrogel beads at 303 K.

Fig. 7 shows the MG adsorption isotherms of the hydrogel beads. The  $q_e$  values increase with an increase of dye concentration for all the samples. The MG adsorption behavior also has an obvious transition point depending on the dye concentration like MB adsorption. For example, the  $q_e$  values of CS1N1 increase from 151.7 to 245.5  $\text{mg g}^{-1}$ , whereas the dye concentration increases from 70.9 to 236.4  $\text{mg L}^{-1}$ . Afterward, the  $q_e$  values slightly increase from 245.5 to 247.4  $\text{mg g}^{-1}$  with the dye concentration from 236.4 to 431.6  $\text{mg L}^{-1}$  at the second stage. The fitting results of Langmuir and Freundlich models are shown in Fig. 8, and the values of isotherm constants are given in Table 3. Overall, correlation coefficient for the Langmuir isotherm model is higher than that for the Freundlich isotherm model. So the Langmuir adsorption model is more suitable to describe the adsorption of MG onto CS and CS-HNTs hydrogel beads, which implies the monolayer coverage of MG.

### 3.5. Adsorption kinetics

The effects of HNTs on the adsorption behavior of chitosan were investigated using MB and MG as model dyes in aqueous solution. Fig. 9 shows the influence of adsorption time on the dye adsorption capacity for different beads. The adsorption curves of MB for all the samples can be divided into two parts: an initial rapid adsorption stages within a short time and next a slow adsorption process [49]. The adsorption rates of MB are fast for the hydrogel beads in the first 20 min and then the rates gradually decrease, and the equilibrium point reaches until 40 min. The equilibrium adsorption amount of CS, CS1N1, CS1N4 hydrogel beads is 67.49, 68.92, and 72.60  $\text{mg g}^{-1}$ , respectively, indicating the increased absorption ability with the HNTs loading. Besides the equilibrium adsorption amount, the  $q_t$  value of the composite hydrogel beads is higher than that of pure chitosan in all the time especially at the initial adsorption stage. The adsorption rate of the composite hydrogel is also faster than that of pure chitosan, which can be seen from the slope of the three curves in Fig. 9. The numerous active sites (hydroxyl groups) of HNTs are related to the fast rates of adsorption in the initial period. With active sites gradually occupied by the dyes, the adsorption rates slow down. When the active sites are fully occupied, the adsorption amount cannot increase any more even upon extending the adsorption time, and the adsorption equilibrium reaches at this moment. The color change of the MB solution before and after adsorption by the different beads is shown in Fig. 10. It can be seen that MB is completely removed by the hydrogel beads within 40 min, eventually leaving the colorless and clear supernatant.

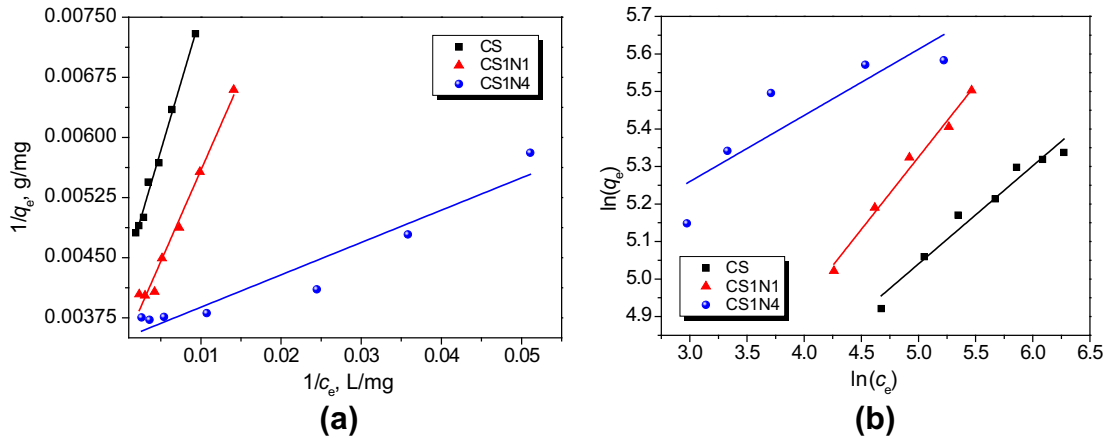


Fig. 8. Langmuir isotherms (a) and Freundlich isotherms (b) for MG adsorption on CS and CS–HNTs hydrogel beads.

**Table 3**  
Langmuir and Freundlich parameters for MG adsorption into chitosan and chitosan–HNTs composite.

Sample	Langmuir parameters			Freundlich parameters		
	$q_{max}$ ( $mg\ g^{-1}$ )	$b$ ( $L\ mg^{-1}$ )	$R^2$	$1/n$	$K_f$ ( $mg\ g^{-1}$ )	$R^2$
CS	243.90	0.0121	0.9910	0.2613	41.83	0.9556
CS1N1	303.03	0.0145	0.9793	0.3855	29.87	0.9826
CS1N4	294.18	0.0910	0.9106	0.1762	113.42	0.6978

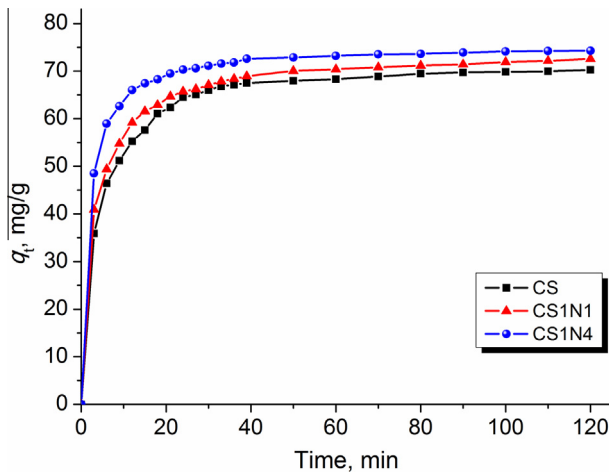


Fig. 9. Influence of adsorption time on the adsorption capacity for methylene blue.

The effect of adsorbent dosage on the adsorption property for MB was also studied. As can be seen from Fig. 11, when the amount of the CS, CS1N1, CS1N4 hydrogel beads increases from 0.002 g to 0.01 g, the removal ratio ( $R$ ) of MB increases from 85.0%, 87.2%, 88.9% to 94.9%, 95.1%, 95.2%, respectively. But the amount of adsorption per unit amount of the hydrogel ( $q_e$ ) reduces from 339.8, 348.7, 355.4 to 75.9, 76.1, 76.2  $mg\ g^{-1}$ . This suggests that with the increase of the amount of hydrogel beads in solution, the removal ratio of dyes gradually increases but the value of  $q_e$  gradually reduces. The reasons of this phenomenon is attributed to the increased active sites for dye adsorption with the increase in the adsorbent amount, leading to the increased removal ratio and decreased concentration of MB remaining in the solution. However, the total amounts of MB keep constant in this system, leading to a decrease in absorption amount per unite adsorbent weight.

In order to investigate the mechanism and characteristics of dye adsorption behavior, the adsorption kinetics of MB on samples were fitted by the pseudo-first-order, pseudo-second-order, and intra-particle diffusion kinetic model. The pseudo-first-order kinetic equation [50] and pseudo-second-order kinetic equation [51] are expressed as:

$$\ln(q_e - q_t) = \ln q_e - k_1 t \tag{4}$$

$$\frac{t}{q_t} = \frac{1}{k_2 q_e^2} + \frac{t}{q_e} \tag{5}$$

where  $q_e$  and  $q_t$  are the amounts of dyes adsorbed on the hydrogel beads ( $mg\ g^{-1}$ ) at equilibrium and time  $t$  (min), respectively;  $k_1$



Fig. 10. Photographs the methylene blue solution before (a) and after (b) adsorption by the chitosan and chitosan–HNTs composite hydrogel beads.

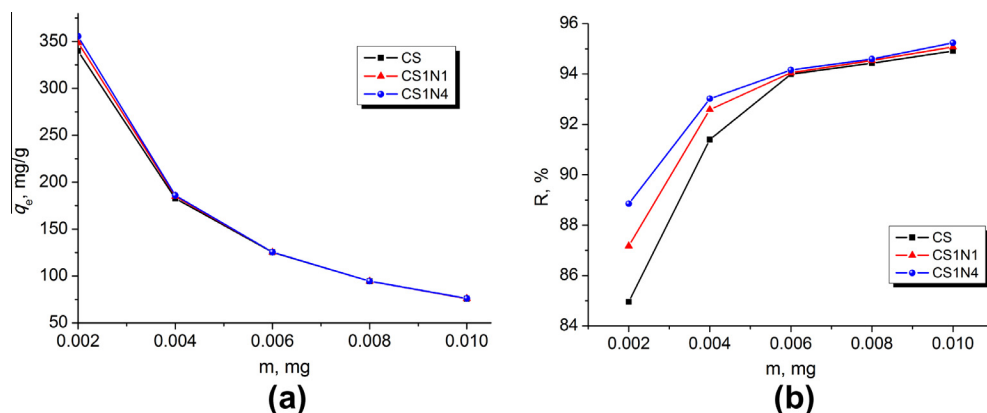


Fig. 11. Influence of adsorbent dosage on the adsorption property for methylene blue. The relationship of adsorbent dosage and  $q_e$  (a), adsorbent dosage and removal ratio (b).

( $\text{min}^{-1}$ ) is the adsorption rate constant of pseudo-first-order model and  $k_2$  ( $\text{g mg}^{-1} \text{min}^{-1}$ ) is the adsorption rate constant of the pseudo-second-order adsorption. To examine the steps involved during adsorption, the intra-particle diffusion model [52] was employed.

$$q_t = k_p t^{1/2} + C \quad (6)$$

where  $C$  is the intercept and  $k_p$  is the intra-particle diffusion rate constant ( $\text{mg g}^{-1} \text{min}^{-1/2}$ ).

The fitting curves are shown in Fig. 12 and the kinetic parameters are calculated and listed in Table 4. According to the values of correlation coefficients, the adsorption kinetics of MB onto the chitosan and its composite beads is better described by the pseudo-second-order model ( $R^2 = 0.9991\text{--}0.9999$ ) than by the

pseudo-first-order model ( $R^2 = 0.8884\text{--}0.9614$ ). Also, the calculated equilibrium adsorption capacity ( $q_{e,\text{cal}}$ ) from the pseudo-second-order model was approximately equal to the experimentally obtained equilibrium adsorption capacity ( $q_{e,\text{exp}}$ ). These results indicate that the adsorption kinetics of MB by the prepared hydrogel beads can be well described by the pseudo-second-order model which implies that the overall rate of the adsorption process is controlled by chemisorption [51] [53]. The intra-particle diffusion model was further employed for examining the adsorption processes involved. The typical plot of  $q_t$  versus  $t^{1/2}$  is shown in Fig. 12(c). It can be seen that there are two adsorption stages. The first one is a rapid stage attributed to the external diffusion of MB from aqueous phase to the external surface of the beads. The other is a slow stage where the gradual adsorption of MB on

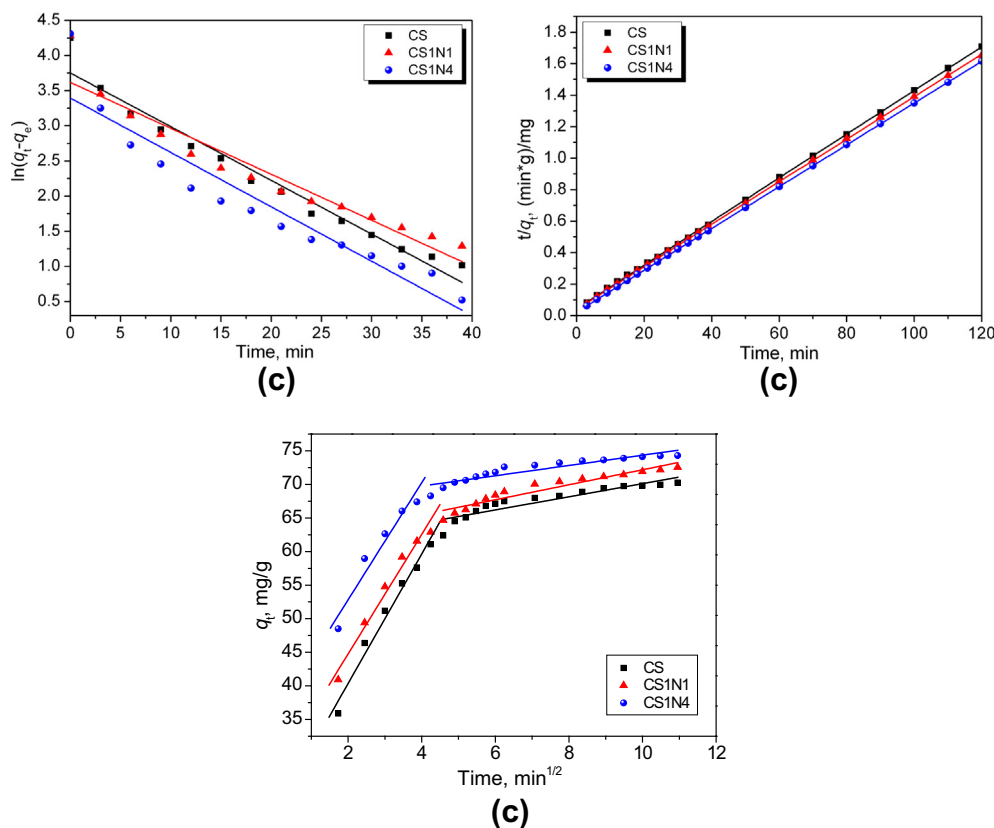
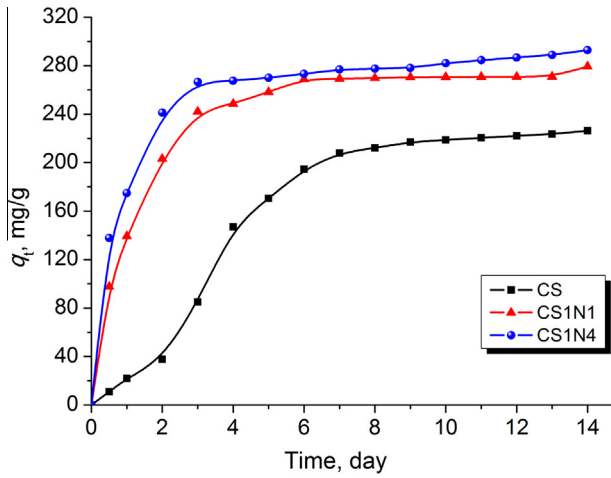


Fig. 12. The linear plot of the pseudo-first-order kinetic model (a), pseudo second-order kinetic model (b), and intra-particle diffusion model (c) for MB adsorption.

**Table 4**  
Kinetic parameters for the adsorption of MB by chitosan and chitosan–HNTs composites by the pseudo-first-order, pseudo-second-order, and intra-particle diffusion model.

Sample	$q_{e,exp}$ (mg g <sup>-1</sup> )	Pseudo-first-order			Pseudo-second-order			Intra-particle diffusion		
		$k_1$ (min <sup>-1</sup> )	$q_{e,cal}$ (mg g <sup>-1</sup> )	$R^2$	$k_2$ (g mg <sup>-1</sup> min <sup>-1</sup> )	$q_{e,cal}$ (mg g <sup>-1</sup> )	$R^2$	$K_p$ (mg g <sup>-1</sup> min <sup>-1/2</sup> )	$C$	$R^2$
CS	67.49	0.0763	42.56	0.9614	0.0044	72.14	0.99991	9.64	21.07016	0.97640
CS1N1	68.92	0.0654	37.27	0.9140	0.0044	74.10	0.99996	8.90	26.94687	0.97445
CS1N4	72.60	0.0774	29.82	0.8884	0.0076	75.37	0.99999	8.71	35.3974	0.94158



**Fig. 13.** Influence of adsorption time on the adsorption capacity for malachite green.

the internal surface of porous hydrogel beads controlled by pore diffusion. MB molecules can pass through the external surfaces and travel within the interior of the hydrogel beads. The adsorption process at least include external diffusion and pore diffusion [53]. The three curves in Fig. 12(c) show  $R^2$  values in the range of 0.94–0.98 which is lower than that calculated by pseudo second order model, indicating the intra-particle diffusion model is not the best model for fitting the MB adsorption process.

Fig. 13 shows the effects of CS, CS1N1, CS1N4 hydrogel beads on the adsorption behavior for MG at different time. CS1N1, CS1N4 hydrogel beads' removal rates of MG are faster within 48 h at the initial period. Then, the rates of adsorption reduce and the equilibrium point is reached in about 7 days. However, CS hydrogel beads' removal rate of MG is slow within 48 h and then the rate of adsorption increases gradually. At last, the equilibrium point is reached in about 7 days, but the adsorption amount is substantially lower than that of CS1N1 and CS1N4 hydrogel beads. The equilibrium adsorption capacity of CS, CS1N1, CS1N4 hydrogel beads is 208.0, 269.2, 276.9 mg g<sup>-1</sup>, respectively. From the photos in Fig. 14, it can be seen the MG solutions nearly become totally colorless and



**Fig. 14.** Photographs the malachite green solution before (a) and after (b) adsorption by the chitosan and chitosan–HNTs composite hydrogel beads.

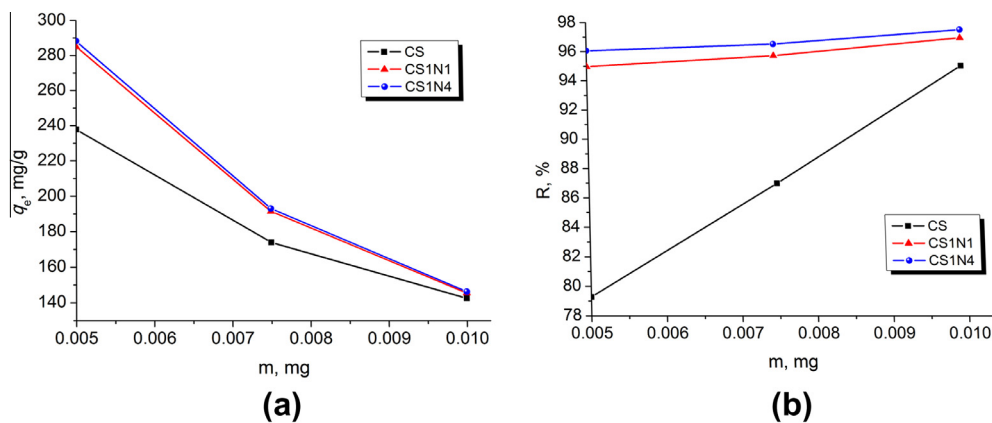


**Fig. 15.** Influence of adsorbent dosage on the adsorption of malachite green. The relationship of adsorbent dosage and  $q_e$  (a), adsorbent dosage and removal ratio (b).

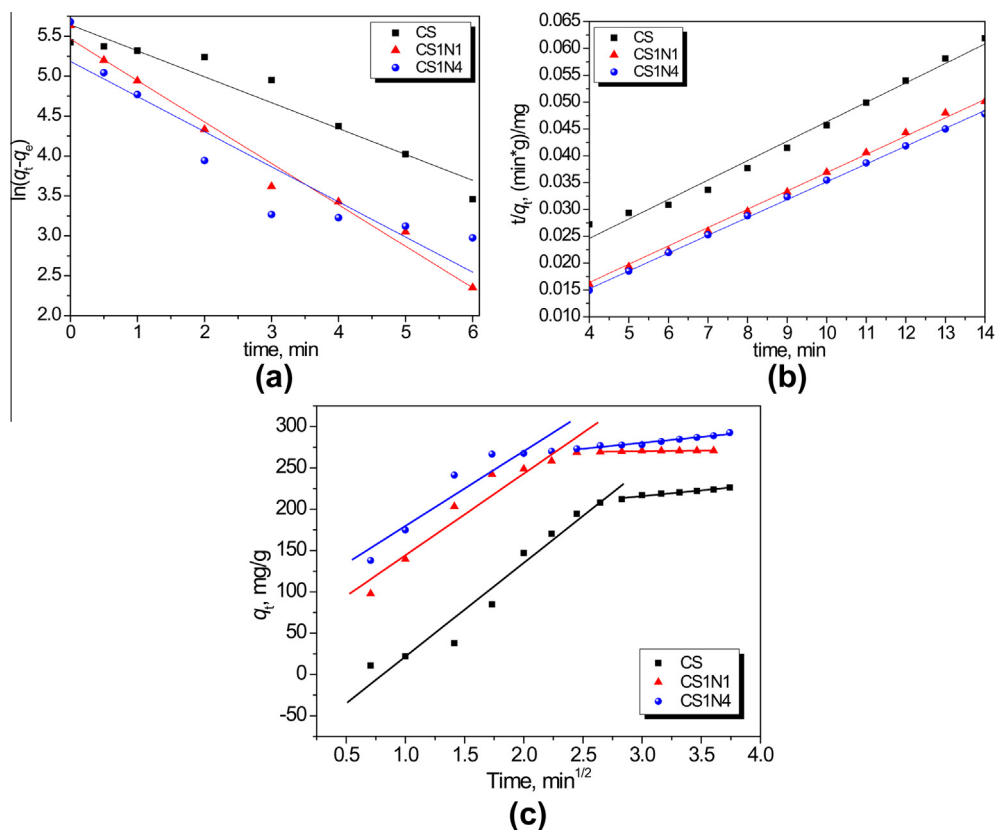


**Fig. 16.** The linear plot of the pseudo-first-order kinetic model (a) and pseudo second-order kinetic model (b) and intra-particle diffusion model (c) for MG adsorption.

**Table 5**

Kinetic parameters for the adsorption of MG by chitosan and chitosan–HNTs composites by the Pseudo-first-order, Pseudo-second-order, and intra-particle diffusion model.

Sample	$q_{e,exp}$ (mg g <sup>-1</sup> )	Pseudo-first-order			Pseudo-second-order			Intra-particle diffusion		
		$k_1$ (min <sup>-1</sup> )	$q_{e,cal}$ (mg g <sup>-1</sup> )	$R^2$	$k_2$ (g mg <sup>-1</sup> min <sup>-1</sup> )	$q_{e,cal}$ (mg g <sup>-1</sup> )	$R^2$	$K_p$ (mg g <sup>-1</sup> min <sup>-1/2</sup> )	$C$	$R^2$
CS	208.0	0.3243	281.74	0.9205	0.0013	276.09	0.98603	113.36	–	0.95262
CS1N1	269.2	0.5189	235.90	0.9804	0.0042	293.17	0.99829	98.75	45.53102	0.93256
CS1N4	276.9	0.4401	178.63	0.8465	0.0057	301.02	0.99939	90.58	89.12997	0.89165

clear after the adsorption by the composite hydrogel beads. However, a certain amount of dye is still present in the solution after adsorption by the pure chitosan beads. Therefore, compared with the MB, the chitosan and its HNTs composite hydrogel beads show higher absorption ability for MG. HNTs can significantly improve the adsorption ability of chitosan for MG.

In order to study the effects of adsorbent dosage on the adsorption of CS, CS1N1, CS1N4 hydrogel beads for MG, 0.005, 0.0075, 0.01 g hydrogel beads were placed in 2 mL MG solution with a concentration of 0.75 g L<sup>-1</sup>. The experimental results are shown in Fig. 15. When the amount of CS, CS1N1, CS1N4 hydrogel beads increases from 0.005 g to 0.01 g, the removal ratio ( $R$ ) of MG increases from 79.3%, 95.0%, 96.1% to 95.0%, 97.0%, 97.5%, respectively and the amount of adsorption reduces from 237.8, 285.0, 288.2 to 142.6, 145.5, 146.3 mg g<sup>-1</sup>, respectively. With the increase of the amount of hydrogel beads in solution, the removal ratio of MG gradually increases. The adsorption efficiency of composite hydrogel beads with HNTs is higher than the pure chitosan hydrogel beads.

The adsorption kinetics of MG by chitosan and chitosan–HNTs composites was also fitted by the pseudo-first-order, pseudo-second-order, and intra-particle diffusion kinetic model. The fitting

curves are shown in Fig. 16 and the kinetic parameters are calculated and listed in Table 5. Consistent with the adsorption of MB, the adsorption kinetics of MG is better described by the pseudo-second-order model than by the pseudo-first-order model. The calculated equilibrium adsorption capacity ( $q_{e,cal}$ ) from the pseudo-second-order model is approximately equal to the experimentally obtained equilibrium adsorption capacity ( $q_{e,exp}$ ). Similar with MB adsorption by the hydrogel beads, the intra-particle diffusion model fitting results also include two adsorption stages, i.e. external diffusion and internal pore diffusion. Also, the CS1N4 shows the highest adsorption amount among the samples.

In total, the adsorption experimental results demonstrate that HNTs can significantly accelerate the adsorption process and improve the adsorption ability of chitosan. The chitosan–HNTs composite hydrogel beads have potential applications for the removal of different dyes from aqueous solutions.

### 3.6. Regeneration of chitosan–HNTs composite hydrogel beads

To regenerate the adsorbents, the MB and MG dyes adsorbed on the hydrogel beads were desorbed by NaOH solution and acetone. The reusability of CS and CS–HNTs hydrogel beads for MB and MG

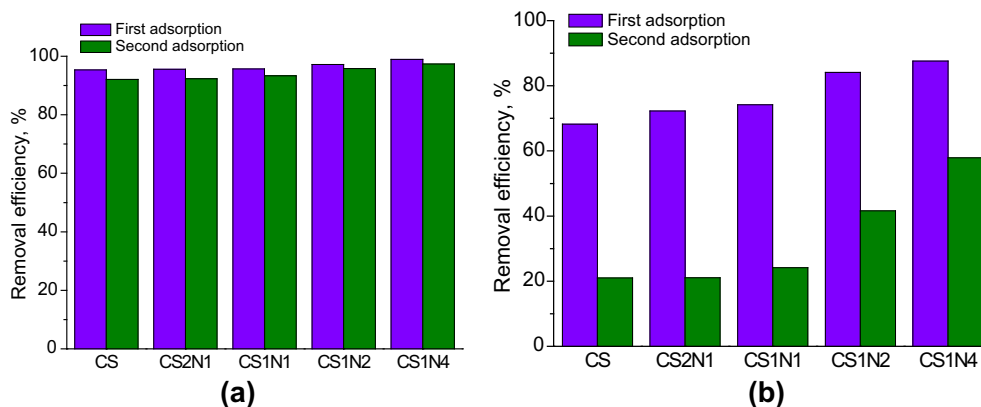


Fig. 17. The reusability of CS and CS-HNTs hydrogel beads for MB (a) and MG (b) removal.

removal as shown in Fig. 17. It can be seen that the removing efficiency of MB at the second adsorption for all the hydrogel beads keeps above 92.0% which is slightly lower than that at the first adsorption. For example, the second removing efficiency of CS1N1 for MB is 93.33% which is only 2.35% lower than that at the first adsorption. The hydrogel beads still show the high efficiency in regeneration, indicating that the hydrogel beads can be well recovered as adsorbents for MB. However, the second adsorption of hydrogel beads on MG dye is moderated possibly due to the relatively weak desorption ability of acetone for MG and the crushing of the hydrogel beads during the adsorption–desorption cycles. With the increase of HNTs, the amount of adsorbed MG at the second adsorption process increases compared with pure chitosan bead. Therefore, the chitosan–HNTs composite hydrogel beads are of great potential as reusable adsorbents of dyes from wastewater.

#### 4. Conclusions

Novel chitosan–HNTs composite hydrogel beads were designed and prepared by the dropping and pH-precipitation method. HNTs can be immobilized by chitosan hydrogel and fully incorporated into the beads' structure. The size of the composite hydrogel beads increases with the HNTs loading. The core of composite beads is filled with a large number of HNTs, while the outer surface of the beads is mainly chitosan by SEM result. TGA shows that chitosan and HNTs are compatible and the thermal stability of the hydrogel beads is remarkably enhanced by HNTs. Both Langmuir isotherm and Freundlich isotherm models can fit the isotherm absorption data well for MB adsorption. As adsorbents for removal of MB and MG from aqueous solutions, the composite hydrogel beads show accelerated adsorption process and improved adsorption ability compared with the pure chitosan hydrogel bead. With the increase of the amount of hydrogel beads in solution, the removal ratio of dyes gradually increases but the absorption amount per unit adsorbent weight reduces. The adsorption kinetics closely follows pseudo-second order model. All the hydrogel beads exhibit a well regeneration property especially for MB adsorption (above 92.0%). Therefore, it can be expected to produce a good wastewater treatment material with unique structures and higher adsorption properties through the synergy of organic chitosan and inorganic HNTs.

#### Acknowledgements

This work was financially supported by the Guangdong Natural Science funds for distinguished young scholar (S2013050014606),

the foundation for the author of Guangdong Excellent Doctoral Dissertation (sybzzxm201220), the project of regional demonstration for Guangdong Ocean Economic Innovative Development (GD2012-B03-009), the Special Fund for Ocean-Scientific Research in the public interest (201405105), and the key project of Department of Education of Guangdong Province (cxzd1108).

#### Reference

- [1] Y. Xing, X.M. Sun, B.H. Li, *Polym. Eng. Sci.* 49 (2009) 272–280.
- [2] V.K. Gupta, *J. Environ. Manage.* 90 (2009) 2313–2342.
- [3] H.S. Rai, M.S. Bhattacharyya, J. Singh, T.K. Bansal, P. Vats, U.C. Banerjee, *Crit. Rev. Environ. Sci. Technol.* 35 (2005) 219–238.
- [4] E. Guibal, E. Touraud, J. Roussy, *World J. Microbiol. Biotechnol.* 21 (2005) 913–920.
- [5] M. Rinaudo, *Prog. Polym. Sci.* 31 (2006) 603–632.
- [6] Y. Zhang, M.Q. Zhang, *J. Non-Cryst. Solids* 282 (2001) 159–164.
- [7] G. Crini, *Bioresour. Technol.* 97 (2006) 1061–1085.
- [8] W.S.W. Ngah, L.C. Teong, M.A.K.M. Hanafiah, *Carbohydr. Polym.* 83 (2011) 1446–1456.
- [9] M.Y. Chang, R.S. Juang, *J. Colloid Interface Sci.* 278 (2004) 18–25.
- [10] W.H. Cheung, Y.S. Szeto, G. McKay, *Bioresour. Technol.* 98 (2007) 2897–2904.
- [11] M.S. Chiou, H.Y. Li, *Chemosphere* 50 (2003) 1095–1105.
- [12] G. Crini, P.-M. Badot, *Prog. Polym. Sci.* 33 (2008) 399–447.
- [13] C. Gerente, V.K.C. Lee, P. Le Cloirec, G. McKay, *Crit. Rev. Environ. Sci. Technol.* 37 (2007) 41–127.
- [14] L. Jin, R.B. Bai, *Langmuir* 18 (2002) 9765–9770.
- [15] F.C. Wu, R.L. Tseng, R.S. Juang, *Water Res.* 35 (2001) 613–618.
- [16] B. Liu, D. Wang, G. Yu, X. Meng, *J. Ocean Univ. China* 12 (2013) 500–508.
- [17] M. Darder, M. Colilla, E. Ruiz-Hitzky, *Appl. Clay Sci.* 28 (2005) 199–208.
- [18] S.H. Hsu, M.C. Wang, J.J. Lin, *Appl. Clay Sci.* 56 (2012) 53–62.
- [19] C.Y. Tang, N.X. Chen, Q. Zhang, K. Wang, Q. Fu, X.Y. Zhang, *Polym. Degrad. Stab.* 94 (2009) 124–131.
- [20] X. Yang, Y. Tu, L. Li, S. Shang, X.-M. Tao, *ACS Appl. Mater. Interfaces* 2 (2010) 1707–1713.
- [21] S. Chatterjee, M.W. Lee, S.H. Woo, *Bioresour. Technol.* 101 (2010) 1800–1806.
- [22] Y. Wang, X. Liu, H. Wang, G. Xia, W. Huang, R. Song, *J. Colloid Interface Sci.* 416 (2014) 243–251.
- [23] P. Monvisade, P. Siriphannon, *Appl. Clay Sci.* 42 (2009) 427–431.
- [24] G.J. Copello, A.M. Mebert, M. Raineri, M.P. Pesenti, L.E. Diaz, *J. Hazard. Mater.* 186 (2011) 932–939.
- [25] E. Joussein, S. Petit, J. Churchman, B. Theng, D. Righi, B. Delvaux, *Clay Miner.* 40 (2005) 383–426.
- [26] S.R. Levis, P.B. Deasy, *Int. J. Pharm.* 243 (2002) 125–134.
- [27] D.G. Shchukin, G.B. Sukhorukov, R.R. Price, Y.M. Lvov, *Small* 1 (2005) 510–513.
- [28] Y.M. Lvov, D.G. Shchukin, H. Mohwald, R.R. Price, *ACS Nano* 2 (2008) 814–820.
- [29] M. Liu, Z. Jia, D. Jia, C. Zhou, *Prog. Polym. Sci.* 39 (2014) 1498–1525.
- [30] M. Du, B. Guo, D. Jia, *Polym. Int.* 59 (2010) 574–582.
- [31] Z.X. Jia, B.C. Guo, D.M. Jia, *J. Nanosci. Nanotechnol.* 14 (2014) 1758–1771.
- [32] Z. Ma, J. Wang, X. Gao, T. Ding, Y. Qin, *Prog. Chem.* 24 (2012) 275–283.
- [33] M. Zhao, P. Liu, *Microporous Mesoporous Mater.* 112 (2008) 419–424.
- [34] L. Liu, Y.Z. Wan, Y.D. Xie, R. Zhai, B. Zhang, J.D. Liu, *Chem. Eng. J.* 187 (2012) 210–216.
- [35] M. Liu, C. Wu, Y. Jiao, S. Xiong, C. Zhou, *J. Mater. Chem. B* 1 (2013) 2078.
- [36] M. Liu, Y. Zhang, C. Wu, S. Xiong, C. Zhou, *Int. J. Biol. Macromol.* 51 (2012) 566–575.
- [37] G. Cavallaro, A. Gianguzza, G. Lazzara, S. Milioto, D. Piazzese, *Appl. Clay Sci.* 72 (2013) 132–137.
- [38] H. Yan, L.Y. Yang, Z. Yang, H. Yang, A.M. Li, R.S. Cheng, *J. Hazard. Mater.* 229 (2012) 371–380.

- [39] C.A. Basar, *J. Hazard. Mater.* 135 (2006) 232–241.
- [40] M.J. Iqbal, M.N. Ashiq, *J. Hazard. Mater.* 139 (2007) 57–66.
- [41] H. Yang, S. Hua, W. Wang, A. Wang, *Iran. Polym. J.* 20 (2011) 479–490.
- [42] Y.F. Chen, Y.T. Zhang, H.Q. Zhang, J.D. Liu, C.H. Song, *Chem. Eng. J.* 228 (2013) 12–20.
- [43] C.M. Dick, J.J. Liggat, C.E. Snape, *Polym. Degrad. Stab.* 74 (2001) 397–405.
- [44] M. Darder, M. Lopez-Blanco, P. Aranda, A.J. Aznar, J. Bravo, E. Ruiz-Hitzky, *Chem. Mater.* 18 (2006) 1602–1610.
- [45] H.-B. Yao, Z.-H. Tan, H.-Y. Fang, S.-H. Yu, *Angew. Chem. Int. Ed.* 49 (2010) 10127–10131.
- [46] I. Langmuir, *J. Am. Chem. Soc.* 40 (1918) 1361–1403.
- [47] H. Freundlich, *Trans. Faraday Soc.* 28 (1932) 195–201.
- [48] H. Tang, W. Zhou, L. Zhang, *J. Hazard. Mater.* 209–210 (2012) 218–225.
- [49] S. Chatterjee, S.H. Woo, *J. Hazard. Mater.* 164 (2009) 1012–1018.
- [50] S. Lagergren, *Kungliga Svenska Vetenskapsakademiens Handlingar* 24 (1898) 1–39.
- [51] Y.-S. Ho, G. McKay, *Process Biochem.* 34 (1999) 451–465.
- [52] S.J. Allen, G. McKay, K.Y. Khader, *Environ. Pollut.* 56 (1989) 39–50.
- [53] R. Wang, X. Cai, F. Shen, *Appl. Surf. Sci.* 305 (2014) 352–358.